Bioelectrochemistry 140 (2021) 107732

Contents lists available at ScienceDirect

Bioelectrochemistry

journal homepage: www.elsevier.com/locate/bioelechem

Electrochemical device based on nonspecific DNAzyme for the high-accuracy determination of Ca^{2+} with Pb^{2+} interference

Hui Wang [a,1], Qingyao Luo [a,1], Yiguang Zhao [a], Xuemei Nan [a], Fan Zhang [a,d], Yaping Wang [a], Yue Wang [a,c], Dengke Hua [a], Shanshan Zheng [a], Linshu Jiang [b], Liang Yang [a,*], Benhai Xiong [a,*]

[a] State Key Laboratory of Animal Nutrition, Institute of Animal Science, Chinese Academy of Agricultural Sciences, Beijing 100193, PR China
[b] School of Animal Science and Technology, Beijing Agricultural University, Beijing Key Laboratory of Dairy Nutrition, Beijing 102206, PR China
[c] College of Animal Science and Technology, Northwest A&F University, Yangling 712100, PR China
[d] State Key Laboratory of Animal Nutrition, College of Animal Science and Technology, China Agricultural University, Beijing 100193, PR China

ARTICLE INFO

Article history:
Received 10 October 2020
Received in revised form 17 December 2020
Accepted 19 December 2020
Available online 29 December 2020

Keywords:
Field-effect transistor
Biosensor
DNA
Calcium ion
Lead ion
Mathematical model
Cow milk
Water

ABSTRACT

Calcium is one of the most abundant and indispensable elements in biology, as it is a vital component of nerves, bones, and muscles and maintains the excitability of normal neuromuscular muscles. However, it may be harmful to the human body and even damage the organs if the calcium content exceeds the standard value by several times. To evaluate the level of calcium ions (Ca^{2+}), an electrochemical biosensor (FET/SWNTs/Cazyme) was developed using a nonspecific DNAzyme with high stability, which combined the unique advantage of field-effect transistors and single-walled carbon nanotubes, while being easy-to-use and having excellent sensitivity. The incubation time and voltage after optimization were 15 min and +0.02 V. The nonspecific DNAzyme-based biosensor was sensitive to Ca^{2+}, but it was also interfered with by Pb^{2+}, which affected the detection accuracy. To solve this shortcoming, an electrochemical device was proposed, in which FET/SWNTs/Cazyme combined with other specific biosensors for Pb^{2+}, and then established some data processing models were established through support vector machine regression (SVMR) and artificial neural network fitting (ANNF). For the optimal SVMR, the electrochemical device can determine the Ca^{2+} concentration in the range of 7.5–1000 μM with a detection limit of 5.48 μM. Finally, the prepared electrochemical device was employed to detect the Ca^{2+} in different milk and water samples.

1. Introduction

Calcium is one of the most abundant and indispensable trace elements in biology [1,2]. It is an essential component for bones and teeth and is also involved in the metabolism of nerves, and muscles that can maintain the excitability of normal neuromuscular muscles [3]. If the daily diet does not provide enough calcium element for a long time, it might cause the abnormal circulation of calcium in the body of the organism [4]. The organism will mobilize calcium from bone or teeth, leading to some severe diseases, such as rickets [5], Crohn's disease [6], celiac disease [7], and osteoporotic fracture in middle-aged individuals [8]. Meanwhile, excessive calcium supplementation affects the absorption of iron and zinc [9]. For example, hypercalcemia disorder typically has symptoms such as abnormal heart rhythm, kidney stones, bone pain, or weakness [10].

Milk is rich in active calcium, vitamin D, and amino acids to meet the requirements of human growth [11]. Among them, calcium is generally found in an amount of approximately 100–130 mg/100 mL, and milk is the best source of calcium because it can be absorbed easily by the human body [12,13]. Presently, there are various brands of milk on the market with the increasing growth of functional dairy. The calcium content in dairy products is an essential indicator of nutritional evaluation [14]. Moreover, the calcium content in water is one of the most critical indicators of water quality [15]. According to the Water Quality Association [16], the water can be classified as soft water, medium, hard water, and extremely hard water based on the levels of calcium and magnesium. Drinking hard or extremely hard water for a long time may damage skin and accelerate aging, causing damage to cardiovascular, nervous, urinary hematopoiesis, and other systems. Consequently, it is of certain necessity and practical value to determine of calcium concentrations in milk and water.

Currently, there are many different methods for the calcium determination, including chemical titration [17], flame atomic absorption spectrometry [18], inductively coupled plasma emis-

* Corresponding authors.
E-mail addresses: yangliang@caas.cn (L. Yang), xiongbenhai@caas.cn (B. Xiong).
[1] Equal Contribution.

https://doi.org/10.1016/j.bioelechem.2020.107732
1567-5394/

sion spectrometry [19], ion-selective electrodes [20], photoacoustic spectroscopy technology [21], Raman spectroscopy [22] and electrochemical sensors [23,24]. Most of them have high anti-noise performance and detection precision, however, their pretreatments are complex, and they are also time-consumption, costly, and require high skill or valuable equipment. Electrochemical sensors provide a powerful tool for the quantitative or semi-quantitative detection of trace calcium. This method and its equipment are very simple and easy to master, and detection stability exists in single sensor detection but with relatively low detection precision. Nevertheless, it can meet the requirements of rapid detection in daily life, which has potential applications in the future [25,26].

Developing DNA-based biomaterials has mainly provided many different mechanisms for metal sensing in the past two decades. RNA-cleaving DNAzyme-based sensors are cost-effective to produce, much more stable than protein- or RNA-based enzymes, which are superior to aptamer-based sensors [25–29], particularly with regards to the detection time. many DNAzyme-based biosensors have been explored to determine the metal ions, such as Na^+ [30], K^+ [31], Ag^+ [32], Cd^{2+} [33], Hg^{2+} [34], Pb^{2+} [35], Mg^{2+} [36], Zn^{2+} [37], Cu^{2+} [38], Ca^{2+} [39,40], and UO_2^{2-} [41]. However, some metal ions, especially Ca^{2+}, lack the specific DNAzyme that can be cleaved or interfered with by other ions. It is a challenging analytical task because these DNAzymes have difficulty distinguishing specific metal ions from complex samples with high accuracy. Liu group [42] reported a fluorescent biosensor using a nonspecific DNAzyme to detect the Ca^{2+} concentration. They tried to use 6-mercapto-1-hexanol to couple with Pb^{2+}, which restrains the cleavage activity. Even though the proposed method can decrease the interference from Pb^{2+}, it is still difficult to quantitatively determine the concentration of Ca^{2+} quantitatively using a single biosensor.

In this work, an electrochemical device made up of a biosensor array associated with machine learning algorithms to solve the limitation of nonspecific DNAzyme for the Ca^{2+} determination. The biosensor array consisted of two different biosensors, which were fabricated using a field-effect transistor and single-walled carbon nanotubes to improve the sensing performance. Using an electrochemical device allows the exploitation of all the information from its biosensors, including the cross-sensitivity and interference from Pb^{2+}, to create a calibration model able to successfully predict Ca^{2+} concentration.

2. Experimental

2.1. Reagents

6-Mercapto-1-hexanol (MCH, 97%) was purchased from Beijing Wokai Biotechnology Co., Ltd (China). Ethanolamine (EA, 99%) and Tween 20 were bought from Sigma Aldrich (USA). 3-Aminopropyltriethoxysilane (APTES, 99%) was provided by Shanghai Aladdin Biochemical Technology Co., Ltd (China). 1-Pyrenebutanoic acid succinimidyl ester (PBASE) was obtained from Thermo Fisher Scientific (China). Single-walled carbon nanotube solution (SWNT, 0.01 mg/mL) was obtained from NanoIntegris Inc. (USA). The standard stock solutions of Ca^{2+} and Pb^{2+} were offered by China National Research Center for Reference Materials (Beijing) and diluted to the required concentrations. Potassium nitrate (KNO_3), sodium nitrate ($NaNO_3$), zinc nitrate ($Zn(NO_3)_2$), copper nitrate ($Cu(NO_3)_2$), iron nitrate ($Fe(NO_3)_3$), magnesium nitrate ($Mg(NO_3)_2$), sodium sulfate (Na_2SO_4), sodium phosphate (Na_3PO_4), sodium chloride(NaCl) and dimethylformamide (DMF) were acquired from Sinopharm Chemical Reagent Beijing Co., Ltd (China). 3-Morpholine propanesulfonic acid (MOPS), sodium hydroxide (NaOH) and ethylenediamine tetraacetic acid (EDTA) were obtained from the Shanghai Mackin Biochemical Technology Co., Ltd (China). The rest of the reagents were of analytical grade without further purification, and ultrapure water from a Millipore Milli-Q system was used throughout the experiment.

The DNA used in this experiment was ordered from the Trilink Bio Technologies in San Diego, CA (USA) and is listed in Table 1. The dried powder was dissolved to 100 nM using sterilized water, and the concentration using a UV spectrometer at 260 nm.

2.2. Apparatus

A CHI 760E electrochemical workstation (CHInstruments, USA) was used to measure the current–voltage (I-V) at room temperature, which the voltage was ranging from −0.2 V to +0.2 V (step +0.01 V). The source as working electrode, the drain as the counter electrode, and the Ag/AgCl as the reference electrode were connected to CHI 760E electrochemical workstation. The UV–Vis absorption spectrum was recorded by DU-800 UV visible spectrophotometer (Beckman Coulter, USA), which was scanned from 200 nm to 800 nm. A high-speed centrifuge (TGL-16C) was purchased from Shanghai Anting Scientific Instrument Factory (China). The vortex mixer (M.L.1-Genie2) was provided by the Beijing Zhuochuan Electronic Technology Co., Ltd (China). An electric tubular furnace (YG-1206) was purchased from Shanghai Yuzhi Electromechanical Equipment Co., Ltd. (China).

2.3. Modification of electrochemical device

Electrochemical device consisted of two biosensors (FET/SWNTs/Cazyme and FET/SWNTs/Pbzyme), which was fabricated using a field-effect transistor (FET) on a high doped p-type silicon wafer through UV lithography, silicon etching, and soft lithography. The drain and source electrode was decorated with 20 nm-thick Cr layer and 180 nm-thick Au layer, which was 10 μm in width and length. As shown in Fig. 1, the biosensor was fabricated using the follows: (1) FET was respectively rinsed with acetone, isopropanol and ammonia to remove organic and inorganic residues; (2) the gap between source and drain was immersed in APTES for 30 min, and then flushed with ultra-pure water; (3) SWNTs solution was covered on the gap for 60 min and rinsed the residual using ultra-pure water, which was further annealed in oven at 250 °C; (4)FET/SWNTs was immersed in 10 mM MCH solution prepared in ethanol for 60 min to block the gold surface, and then put into 6 mM PBASE solution prepared in DMF that can immobilized PBASE through π–π bond formation between pyrene and SWNTs; (5)PBASE-modified SWNTs were incubated with 100 μM of amine-labeled CS-DNA (8 h) in phosphate buffer (PB, 10 mM, pH 7.4) overnight at 4 °C; (6) the device was further treated with 0.1 mM EA to block excess ester groups of PBASE and 0.1% Tween 20 to prevent nonspecific binding to SWNT; (7)CS-DNA captured on the SWNT surface was hybridized with DNAzyme by incubating with 100 μM DNAzyme in PB for 2 h at room temperature to form a DNA duplex.

2.4. Sensing protocol

To determinate Ca^{2+} concentration, the sensing protocol was performed as following steps: The biosensor array was covered with MOPS (pH 6.95) for a while and was measured the current at +0.02 V. Next, the biosensor array was incubated with the processed sample for 15 min at room temperature. Next, the biosensor array was rinsed with sufficient buffer solution several times to remove the residue of Ca^{2+} and Pb^{2+} residues. Then, the biosensor array was covered with buffer solution and was measure the resistance again.

Table 1
DNA oligonucleotides used in this study.

Name	Sequence and modifications (from 5′-terminus)
CS-DNA	/AmMC6/CGG TAG AAG GrAT ATC ACT GAG CAC
CO-DNA	/AmMC6/CGG TAG AAG GAT ATC ACT GAG CAC-
Pbzyme	GTG CTC GAT AT GC CGC CGC GAT GAA GTC TAC CG
Cazyme	GTG CTC AGT GAT TGT TGG AAT CGC TCA TGC GAC ACT CTT TTC TAC CG

The relative resistance was calculated using the following equation:

$$Relative\ resistance = (R_0 - R)/R_0 \times 100\% \quad (1)$$

where R_0 is the initial resistance value, and R is the resistance after the exploration of the extracted solution. Finally, the relative resistances of the biosensor array were processed by the established model to obtain the Ca^{2+} concentration.

2.5. Milk sample extract preparation

Retail packaged cow milk was obtained from a local supermarket (Beijing, China). The whole milk was analyzed using an established method [33]. Briefly, (1) a mixture of 10 g of milk sample and 1 mL of HNO_3 solution was added into a crucible for 30 min and then evaporated to dryness by using electric furnace; (2) the sample was transferred to muffle furnace, ashed at 490 °C for 5 h and cooled down at room temperature; (3) the sample was dissolved with HNO_3 for serval times; (4) the extracted solution was transferred to the 25.0 mL volumetric flask, and added water to the scale; (5) 5 mL of the obtained solution was placed into a 50 mL volumetric flask and was fixed the volume with MOPS buffer. The water sample was filtered using a 0.22 μm membrane to remove large particles and then added MOPS buffer to adjust pH.

2.6. Regression model

2.6.1. Support Vector Machine regression

Support vector machine regression (SVMR) [43] is an important branch of support vector machines for the finite samples and has been widely used to establish a calibration model. This method maintains all the main features that characterize the algorithm (maximal margin), which guarantees the structural risk minimization and finds a compromise between the accuracy of approximation to a given data and the complexity of the approximation function. SVMR builds a linear regression function between data set x and the target values y as follows:

$$f(x_i, w) = w \cdot x_i + b \quad (2)$$

where w is the regression coefficient vector and b is the bias term.

To calculate the regression coefficients, SVM regression attempts to minimize the loss function as defined by:

$$|y_i - f(x_i, w)|_\varepsilon = \begin{cases} 0 & if\ |y_i - f(x_i, w)| \le \varepsilon \\ |y_i - f(x_i, w)| - \varepsilon & otherwise \end{cases} \quad (3)$$

where ε var epsilon is the maximum difference between the predicted value and the target value that can be neglected.

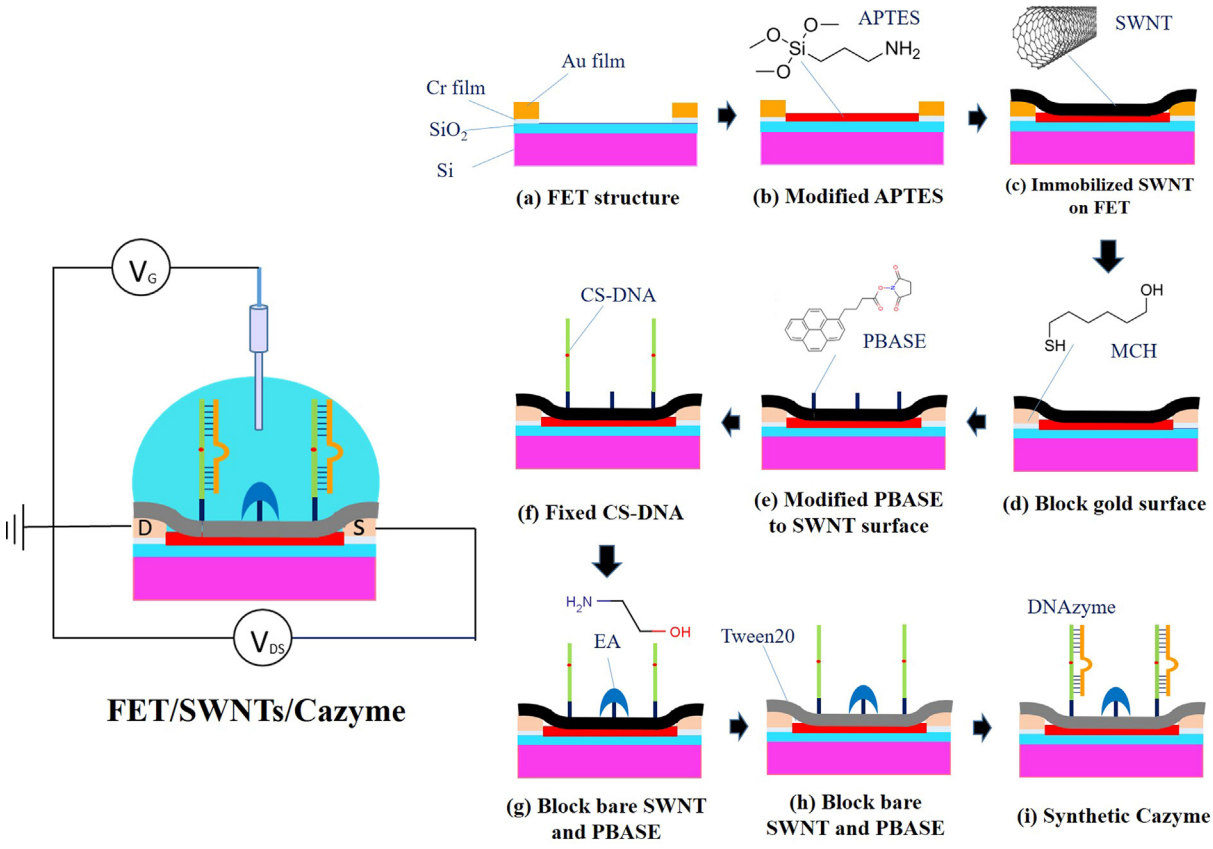

Fig. 1. Illustration of FET functionalized with different materials: (a) FET rinsed with acetone, isopropanol, and ammonia to remove the contaminant; (b) APTES modified on the gap between source and drain to immobilize SWNTs; (c) SWNTs immobilized on FET's surface to conduct the source and drain, and removed the surfactants at high temperature; (d) MCH blocked gold surface though Au-S bond to prevent impurity adsorption; (e) PBASE immobilized on SWNT's surface through π–π bond; (f) Amine-labeled CS-DNA connected to PBASE though peptide bond; (g) EA blocked the unreacted PBASE and bare SWNTs; (g) Tween 20 attached on naked SWNTs' surface; (i) DNAzyme hybridized with CS-DNA to form Cazyme.

2.6.2. Artificial neural network fitting

Artificial neural network fitting [44] is a three-layer forward network composed of an input layer, hidden layer, and output layer. It has the potential to learn input–output correlation by training the input to produce the expected output. The process can be divided into two stages: (1) The first stage is the learning period, in which the state of each calculation unit remains unchanged, and the weights on each line can be modified by learning; (2) the second stage is to work on it, at which time the connection weights are fixed and the state of the calculation unit changes to achieve a certain stable state. The problem to be solved by the neural network is to train the neural network repeatedly through known data to obtain the weighted sum threshold so that the error between the calculated output Y of the neural network and the expected output signal is minimized. A more appropriate way is to minimize the sum of squares of errors.

3. Results and discussion

3.1. Characterizations

Fig. 2 shows the UV–visible spectrum of quartz before and after decoration with SWNTs, PBASE, and Cazyme (CS-DNA/DNAzyme with excellent optical properties. The blank quartz was selected as the background so that there was no peak in the absorption spectrum. After SWNTs modification, an obvious peak was found at 260 nm, and the absorption spectrum in the whole range improved significantly. For PBASE, two absorption peaks were located at 240 nm and 270 nm, ascribing to PBASE immobilized on the SWNTs surface through π- π interactions. When Cazyme was functionalized with FET/SWNTs/PBASE, only one strong absorption peak was found on the curve, which was located at 275 nm. The main reason was that the absorption peak of Cazyme overlapped with the two weak peaks of PBASE [45].

SWNTs were modified with MCH, PBASE, CS-DNA, EA, TWEEN 20, and DNAzyme, which will affect the conductivity or impedance. As shown in Fig. 3(A), the currents at different voltages decreased and were not prolonged linearly in the view of the positive-type semiconductor of SWNTs. The resistances at different voltages are calculated in Fig. S1 and was highly negatively correlated with the voltage. The resistances at +0.02 V are displayed in Fig. 3(B). The resistance value of SWNTs/FET was approximately 2.3 kΩ.

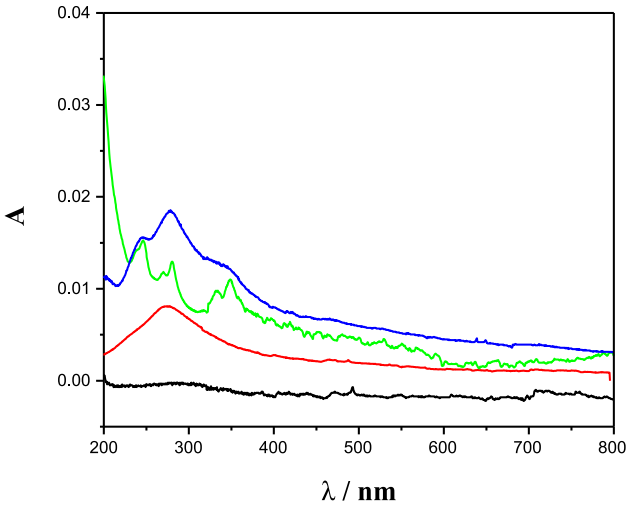

Fig. 2. UV–vis spectrum of quartz modified with SWNTs, PBASE, and Cazyme: Blank Quartz (black), Quartz/SWNTs (red), Quartz/SWNTs/PBASE (green), Quartz/SWNTs/PBASE/Cazyme (dark blue). (For interpretation of the references to color in this figure legend, the reader is referred to the web version of this article.)

After MCH modification, the resistance increased slightly because MCH does not bind with SWNTs directly. For the rest of the reagents and materials, the pyrene of PBASE was decorated on the SWNTs surface through π–π bonds, and EA was used to link to PBASE that do not bind with CS-DNA, and TWEEN20 could block the naked surface of SWNTs to prevent the adsorption of impurities. They were direct or indirect contact with SWNTs, which affected the number of charge carriers in semiconducting SWNTs.

3.2. Optimization

Fig. 4(A) shows that FET/SWNTs/Cazyme was applied to measure the two different Ca^{2+} concentrations (25 μM and 1000 μM), and the relative resistance changed with the incubation time in the range from 3 min to 21 min. It was clear that the relative resistance exhibited a significant linear correlation with the incubation time in the first 12 min. After that, the growth rate of the relative resistance decreased, especially for high Ca^{2+} concentrations, which can be ascribed to that the limited Cazyme on the FET/SWNTs might be cut-off by the Ca^{2+}. To guarantee stability, 15 min was selected as the incubation time in the experiment.

Determining the relative resistance was an effective method to decrease the difference among the biosensors because it was difficult to control the resistances of FET/SWNTs/Cazymes that need to consume more time and energy. To optimize the condition, FET/SWNTs/Cazyme was applied to determine different Ca^{2+} concentrations. Fig. S2(A) and (B) shows the current vs. voltage and resistance–voltage for the different Ca^{2+} concentrations. The current nonlinearly increases with the voltage ranging from −0.2 V to 0.2 V but was linear with the resistance, except for 0 V. The electrochemical properties of FET/SWNTs/Cazyme were affected by the semiconductor SWNTs, and pH 7.4 buffer solution was approximate as a negative voltage. Based on the equation in 2.4, the relative resistances for different Ca^{2+} concentrations were calculated and are shown in Fig. 4(B). For a certain Ca^{2+} concentration, the relative resistances at different voltages showed almost no change. Therefore, +0.02 V was chosen in the experiment to simplify the detection operation.

The cleavage site of CS-DNA is shown in Fig. 4(C). CS-DNA with or without RNA base was made of two different types of FET/SWNTs/Cazyme and FET/SWNTs/Cczyme for three different Ca^{2+} concentrations. For the CS-DNA without RNA base, the relative resistances were changed little before and after exposure to Ca^{2+} solution. The relative resistances of FET/SWNTs/Cazyme were 12.59, 35.43, and 56.69 for the 10 μM, 100 μM, and 1000 μM, respectively. This illustrated that the Ca^{2+}-cleavage site occurred at the position of rA-modified CS-DNA.

To assess the stability, several FET/SWNTs/Cazyme were fabricated by following the protocol in 2.3, which were covered with MOPS buffer and stored in a refridge at 4 °C. Every two days, FET/SWNTs/Cazyme was randomly chosen to measure 500 μM Ca^{2+}, and the results are listed in Fig. 4(D). The relative resistance remained constant at the same Ca^{2+} concentrations in the first five days. Subsequently, the relative resistance started to decrease slightly, indicating that FET/SWNTs/Cazyme was stable in the early five days.

3.3. Selectivity

Selectivity is one of the most important properties of the electrochemical biosensor. For milk and water, many metal ions, including Pb^{2+}, Na^{+}, K^{+}, Mg^{2+}, Cd^{2+}, Zn^{2+}, Cu^{2+}, Fe^{3+}, and Cr^{3+}, might exist in the real sample, which probably affects the detection accuracy. To evaluate the selectivity, FET/SWNTs/Cazyme was employed to measure the different metal ions under the optimal conditions. The detection results are shown in Fig. 5. The relative

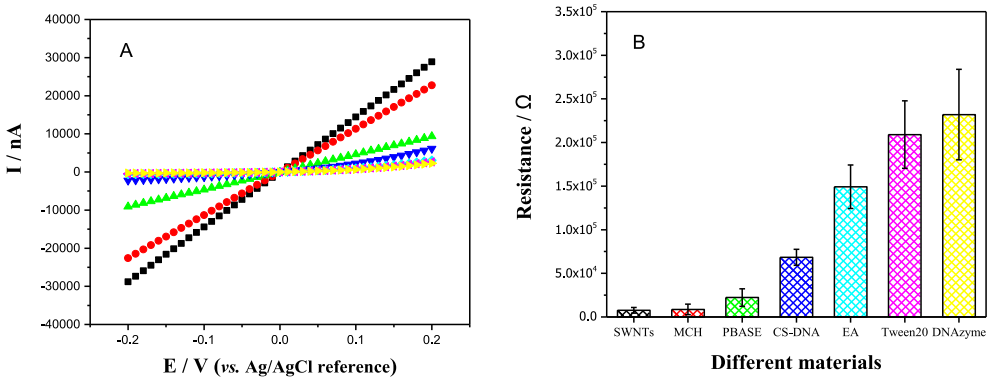

Fig. 3. (A) Current changing with voltage applied bewteen source and drain from −0.2 V to +0.2 V with step +0.01 V and (B) Resistance values between source-drain calculated at V_{DS} = +0.02 V and V_G = 0 V after FET functionalized with different materials: SWNTs (black), MCH (red), PBASE (green), CS-DNA (dark blue), EA (blue), Tween20 (purple) and DNAzyme (yellow). (For interpretation of the references to color in this figure legend, the reader is referred to the web version of this article.)

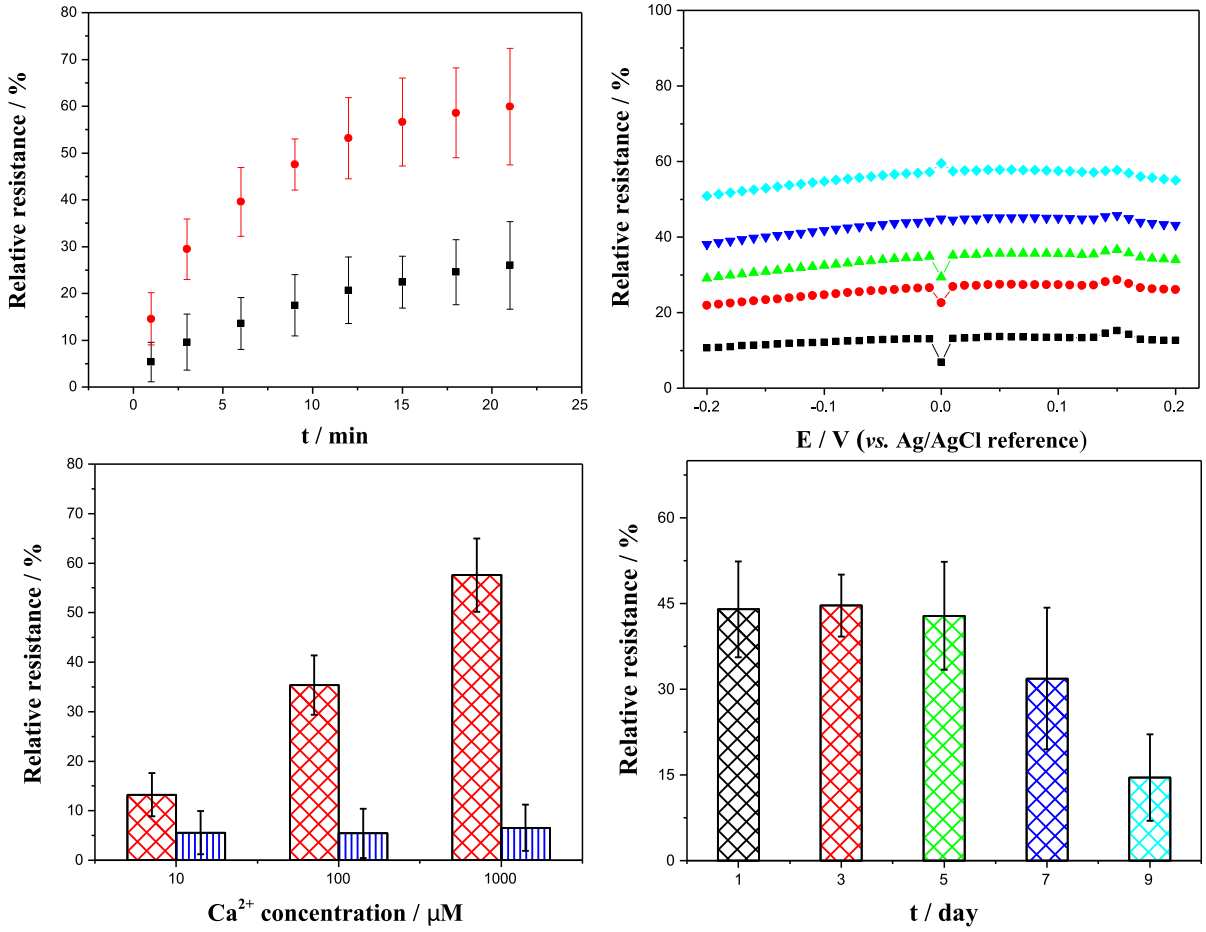

Fig. 4. (A) The relative resistance (the change rate of resistance at different reaction time to resistance at 0 min) of FET/SWNTs/Cazyme changing with incubation time from 3 to 21 min for the 25 μM (black) and 100 μM (red) Ca^{2+}; (B) The relative resistance of FET/SWNTs/Cazyme (the change rate of resistance for different Ca^{2+} concentration to resistance for 0 μM Ca^{2+}) changing with the voltage of for different Ca^{2+} concentrations:10 μM (black), 50 μM (red), 100 μM (green), 500 μM (dark blue) and 10000 μM (blue); (C) Relative resistance affacted by CS-DNA with or without 'rA' for the Ca^{2+} detection that equal to the change rate of FET/SWNTs/Cazyme (red) and FET/SWNTs/Cczyme (dark blue) before and after exposure to different Ca^{2+} concentrations; (D) The relationship between storage time and relative resistance of FET/SWNTs/Cazyme for 500 μM Ca^{2+}. (For interpretation of the references to color in this figure legend, the reader is referred to the web version of this article.)

resistances for Pb^{2+} and Ca^{2+} were much higher than those of the rest of the metal ions. In comparison to the blank buffer solution, the relative resistances of four metal ions (Cu^{2+}, Zn^{2+}, Mg^{2+}, and Fe^{3+}) increased slightly, indicating that most metal ions did not interfere with the FET/SWNTs/Cazyme.

3.4. Mathematical model

3.4.1. Linear regression

FET/SWNTs/Cazyme was applied to investigate the linear range and the detection limit under the optimal conditions. Different

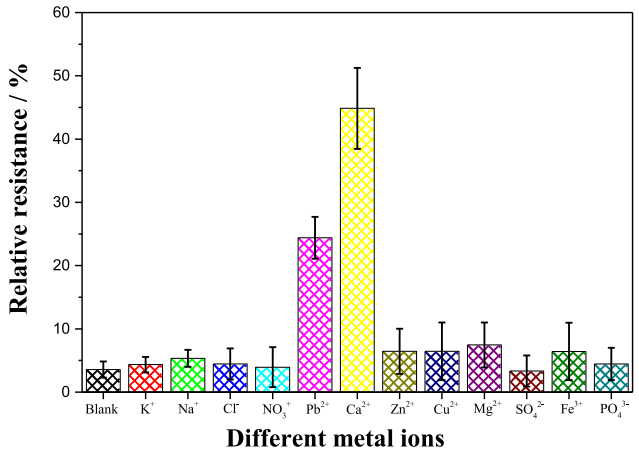

Fig. 5. The relative resistance equal to the resistance change of FET/SWNTs/Cazyme before and after exposure to different co-existing ions (500 μM) for 15 min.

Ca^{2+} concentrations were measured using FET/SWNTs/Cazyme, and the relative resistances at +0.02 V were listed in Fig. 6. When the Ca^{2+} concentration was lower than 7.5 μM, the relative resistance was almost unchanged, which indicated that the CS-DNA was not cleaved by Ca^{2+}. The values of the relative resistance increased with the Ca^{2+} concentrations; the change in the relative resistance exhibited a linear relationship with the logarithm of the Ca^{2+} concentration in the range from 7.5 μM to 1000 μM. The linear regression equation was $Relative\ resistance = -9.4091 + 21.551 log_{10}\left[Ca^{2+}\right](\mu M)$ with a linear regression coefficient of 0.991. The detection limit was calculated as 5.6 μM (S/N = 3).

3.4.2. Nonlinear regression

Due to the poor selectivity of FET/SWNTs/Cazyme, Pb^{2+} might interfere with the detection accuracy in the real sample. To overcome this deficiency, the electrochemical device was established using FET/SWNTs/Pbzyme [46] and FET/SWNTs/Cazyme, in which the detection results were processed using different mathematical models.

The input and output variables were preprocessed using the following equations:

$$Y = log_{10}(C/1000 + 10) - 1$$

$$X = [1, x_1, x_2, {x_1}^2, {x_2}^2, x_1 \times x_2]$$

where C is the concentrations of Ca^{2+} and Pb^{2+}, and x_1 and x_2 are the relative resistances of FET/SWNTs/Cazyme and FET/SWNTs/Pbzyme, respectively.

(1) **Support vector machine regression**

In Fig. 7, there was a data set containing 44 samples. SVM regression was conducted using Matlab software. The X matrix was chosen as the workspace variable, and the Y matrix was selected as the response. Cross-validation was set as 5 folds. After training the data set, the predicted concentration against the true concentration of Ca^{2+} is displayed in Fig. 8. The limit of detection was 5.48 μM. The root mean square error (RMSE), mean square error (MSE), and R-squared were calculated to be 0.16241, 0.026376, and 0.95, respectively.

(2) **ANN model**

As shown in Fig. 9, the ANN model was used for static fitting problems with a standard two-layer feed-forward neural network

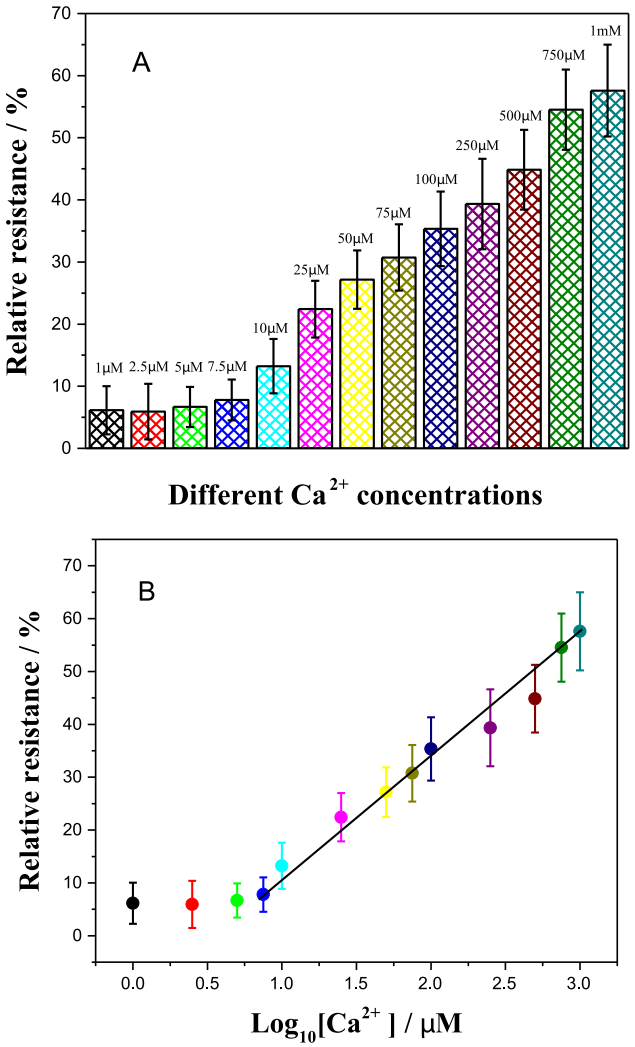

Fig. 6. (A) The relative resistances of FET/SWNTs/Cazyme exposed to different Ca^{2+} concentrations ranging from 1 μM to 1000 μM; (B) The linear relationship between relative resistance and the logarithm of the Ca^{2+} concentration: Relative resistance = $21.551 Log_{10}[Ca^{2+}]$-9.4091 and R^2 = 0.9824.

trained with the Levenberg-Marquardt (LM) algorithm. The procedure was mainly divided into three parts containing an input layer, hidden layers, and an output layer. The X matrix was selected as an input layer, and the corresponding Y matrix was chosen as the output layer. In accordance with a predefined percent of data division, the data set was divided randomly into 70% training, 15% validation, and 15% for testing.

The number of hidden layer nodes depended on the complexity of the approximated function. The optimal number of hidden nodes was related to the number of hidden nodes varying from 6 to 11. The dataset was trained with the Levenberg-Marquardt (LM) algorithm, which was performed when the performance was evaluated by using RMSE, MSE, and R-squared. When the number of hidden nodes was 9, the predicted concentration against the true concentration of Ca^{2+} is exhibited in Fig. 10. The limit of detection was 4.86 μM. An RMSE of 0.386, an MSE of 0.1481, and an R-squared of 0.96 were obtained for the training data set.

To evaluate the effectiveness, R-squared values of the two methods were calculated similarly, but the values of RMSE and MSE R-squared values for the SVM were less than those of the ANN method. The results show that SVM regression method pre-

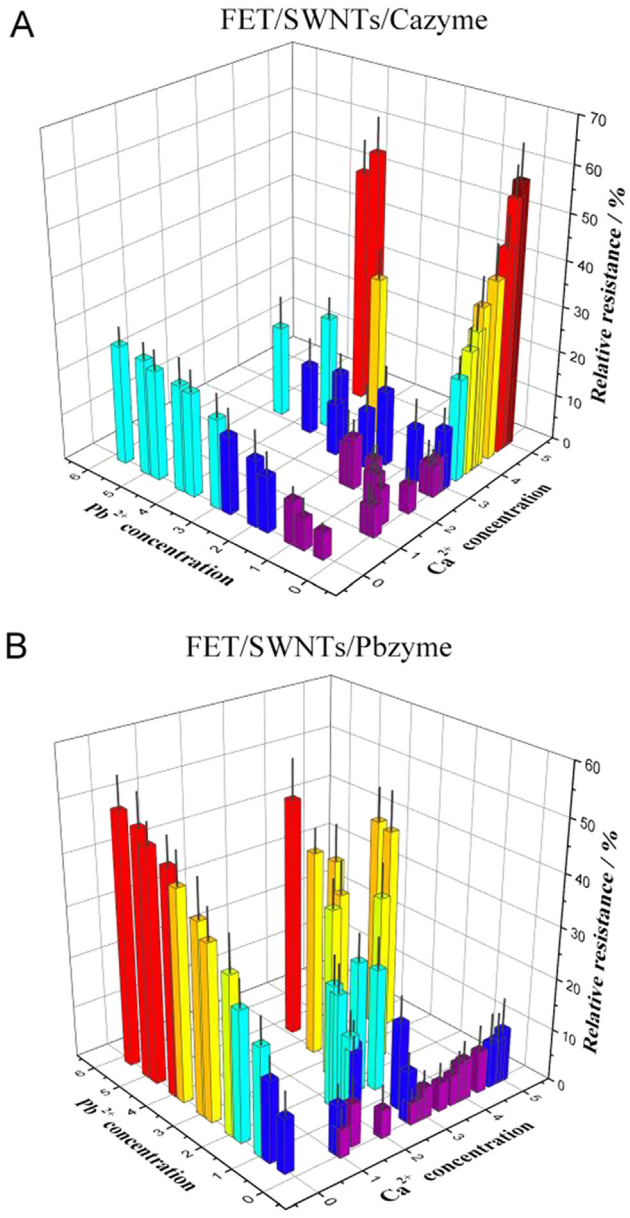

Fig. 7. The relative resistance of FET/SWNTs/Cazyme (A) and FET/SWNTs/Pbzyme (B) after exposure to different mixture solutions of Ca^{2+} and Pb^{2+}. (The concentration ratio of Ca^{2+} vs. Pb^{2+}: 5000–0, 7500–0, 10000–0, 25000–0, 75000–0, 100000–0, 250000–0, 500000–0, 750000–0, 1000000–0; 100–0.5, 250–5, 500–25, 750–50, 1000–250, 5000–500, 10000–5000, 25000–2500, 500000–500000; 100–3.5, 500–35,1000–350, 5000–3500,10000–35000, 15000–350000; and 1000–0.3, 5000–3, 7500–30, 10000–300, 70000–3000, 700000–30000; 0–10, 0–50, 0–100, 0–500, 0–1000, 0–5000, 0–10000, 0–50000, 0–100000, 0–5000000 nM. The error bars indicate standard deviations from five biosensors.

dictors perform better in Ca^{2+} concentration values than the ANN method. The reasons were mainly the follows: (1) SVM regression can obtain a global optimal solution and achieve maximum reliability for the prediction of small samples in practical applications; (2) compared with the ANN model, the SVM algorithm can effectively prevent overfitting, omission learning, and difficulty in determining the network structure. Therefore, SVM was selected as the model to predict the Ca^{2+} concentration.

3.5. The performance comparison

For the Ca^{2+} determination, the detection parameters of different sensors are listed in Table S1. Even though the limit of detection of the proposed method was much higher, the linear range was better than that of the majority of sensors that can meet the requirements of practical application. Compared with most spec-

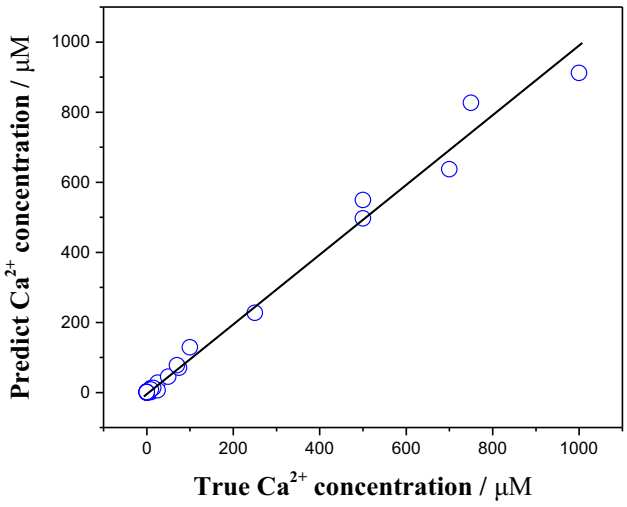

Fig. 8. Predicted Ca^{2+} concentration against true Ca^{2+} concentration using the established SWM model.

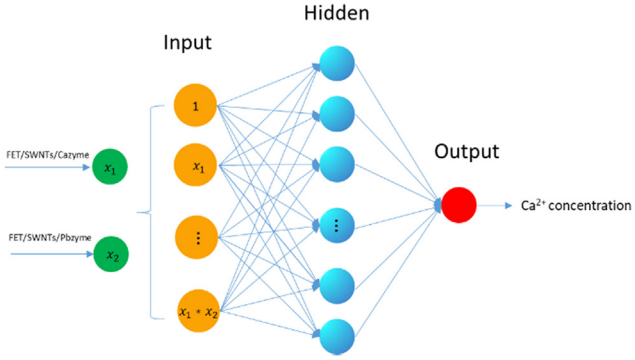

Fig. 9. The overall structure of ANN model. The relative resistance of FET/SWNTs/Cazyme and FET/SWNTs/Pbzyme for different Ca^{2+} concentrations pretreated using the X-matrix as input and then processed LM algorithm with different hidden nodes to predict the Ca^{2+} concentration.

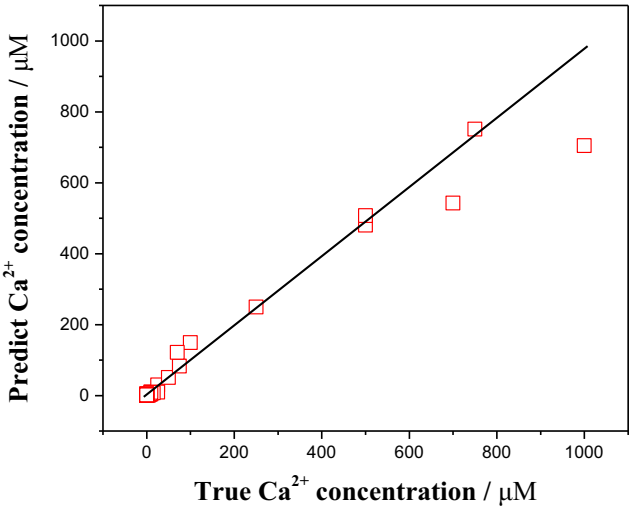

Fig. 10. Predicted Ca^{2+} concentration against true Ca^{2+} concentration using the established ANN model.

Table 2
Ca^{2+} concentration in the real sample determined by the electrochemical device and HPLC.

Sample	Electrochemical device (μM)	HPLC (μM)	Recovery (%)
1	118 ± 8	126	93.65
2	134 ± 12	119	112.61
3	145 ± 10	133	109.02
4	12 ± 2	13	92.31
5	14 ± 1	15	93.33
6	21 ± 2	23	91.30

troscopic methods, the detection time was 15 min, which was relatively modest.

3.6. Analysis of real samples

The whole milk samples (1–3) were bought from the local market, and water samples (4–6) were collected from the tap water, which was pretreated using the protocol in Section 2.4. As shown in Table 2, all the extracted samples were measured using the proposed method and HPLC. The recoveries were ranged from 91.30% to 112.61%, illustrating that the electrochemical device could be efficiently applied to determine Ca^{2+} in milk or water. A *t*-test was used to analyze the results of the two methods, which obtained P = 0.946 > 0.05. It can be concluded that there was no significant difference between the results obtained by the two methods, indicating that the proposed biosensor was accurate and reproducible.

4. Conclusion

In this study, a sensitive electrochemical device using Ca^{2+}-nonspecific RNA-cleaving DNAzyme was developed for Ca^{2+} determination, which has low selectivity with Pb^{2+} interference. For only FET/SWNTs/Cazyme, the linear range was from 7.5 μM to 1000 μM with a detection limit of 5.6 μM. To determine the Ca^{2+} in milk or water with high accuracy, FET/SWNTs/Pbzyme was combined with FET/SWNTs/Cazyme to form a biosensor array, and the detection results were processed using SVMR and ANNR to establish mathematical experiential models. Through comparison, SVM was selected and exhibited good performance to predict the Ca^{2+} concentration. Finally, the prepared electrochemical device was employed to detect the Ca^{2+} in different milk and water samples with good results.

Declaration of Competing Interest

The authors declare that they have no known competing financial interests or personal relationships that could have appeared to influence the work reported in this paper.

Acknowledgments

This work was supported by Research and verification on the theory and electromechanical control technology of precise feeding of livestock and poultry (No. 2016YFD0700205), Key Realm R&D Program of Guangdong Province (No. 2019B020215004 and No. 2019B020215002), Central Public-interest Scientific Institution Basal Research Fund (No. 2019-YWF-YB-10), Science and Technology Innovation Project of Institute of Animal Animal Sciences (No. cxgc-ias-09-1) and Beijing Dairy Industry Innovation Team (No. bjcystx-ny-1).

Appendix A. Supplementary material

Supplementary data to this article can be found online at https://doi.org/10.1016/j.bioelechem.2020.107732.

References

[1] Š. Zamberlin, N. Antunac, J. Havranek, D. Samaržija, Mineral elements in milk and dairy products, Mljekarstvo: časopis za unaprjeđenje proizvodnje i prerade mlijeka 62 (2012) 111–125.
[2] F.S. Al-Fartusie, S.N. Mohssan, Essential trace elements and their vital roles in human body, Indian J. Adv. Chem. Sci. 5 (2017) 127–136.
[3] A.S. Alawad, S.B. Alawadi, I.H. Al-Dujaily, N.B. Alawadi, Trace elements in pregnant women from Babil Province, Iraq, Ann. Trop. Med. Heal. 22 (2019) 64–71, https://doi.org/10.36295/asro.2019.22109.
[4] M.A. Zoroddu, J. Aaseth, G. Crisponi, S. Medici, M. Peana, V.M. Nurchi, The essential metals for humans: a brief overview, J. Inorg. Biochem. 195 (2019) 120–129, https://doi.org/10.1016/j.jinorgbio.2019.03.013.
[5] C.M. Schnitzler, J.M. Pettifor, Calcium deficiency rickets in African adolescents: cortical bone histomorphometry, JBMR plus 3 (2019), https://doi.org/10.1002/jbm4.10169 e10169.
[6] U. Christerson, Å.V. Keita, M.E. Winberg, J.D. Söderholm, C. Gustafson-Svärd, Possible involvement of intracellular calcium-independent phospholipase A2 in the release of secretory phospholipases from mast cells—increased expression in Ileal mast cells of Crohn's disease, Cells 8 (2019) 672, https://doi.org/10.3390/cells8070672.
[7] I.M. Abrudan, B. Kelemen, A.M. Girbovan, C.V. Abrudan, C. Crisan, G. Sur, G. Samasca, The diagnosis of patients with celiac disease and calcium deficiency, Int. J. 4 (2016) 16–18, https://doi.org/10.12691/ijcd-4-1-3.
[8] W. Lin, R. Wang, Calcium status may modify the association of magnesium and potassium intake with heel bone ultrasound attenuation and osteoporotic fracture risk in the European Prospective Investigation into Cancer and Nutrition-Norfolk cohort study, Am. J. Clin. Nutr. 103 (2016) 290, https://doi.org/10.3945/ajcn.115.121400.
[9] R.J. Wood, J.J. Zheng, High dietary calcium intakes reduce zinc absorption and balance in humans, Am. J. Clin. Nutr. 65 (1997) 1803–1809, https://doi.org/10.1093/ajcn/65.6.1803.
[10] P.A. Schenck, D.J. Chew, L.A. Nagode, T.J. Rosol, Disorders of calcium: hypercalcemia and hypocalcemia 4 (2006) 120–194, https://doi.org/10.5772/intechopen.87272.
[11] A. Skwarek, J. Pachucki, T. Bednarczuk, Z. Żurecka, M. Popow, A. Kondracka, Z. Bartoszewicz, Milk-alkali syndrome (MAS) as a complication of the treatment of hypoparathyroidism—a case study, Endokrynol. Pol. 69 (2018) 200–204, https://doi.org/10.5603/ep.a2018.0015.
[12] L. Li, X. Liu, H. Guo, The nutritional ingredients and antioxidant activity of donkey milk and donkey milk powder, Food Sci. Biotechnol. 27 (2018) 393–400, https://doi.org/10.1007/s10068-017-0264-2.
[13] M.E. Walters, R. Esfandi, A. Tsopmo, Potential of food hydrolyzed proteins and peptides to chelate iron or calcium and enhance their absorption, Foods 7 (2018) 172, https://doi.org/10.3390/foods7100172.
[14] H.F.d. Souza, L.A. Borges, J.P.A. Lopes, B.M.A.d. Carvalho, S.H.S. Santos, A.C.d. Almeida, W.J.N. Lima, I.V. Brandi, Elaboration, evaluation of nutritional information and physical-chemical stability of dairy fermented drink with caja-mango pulp, Ciência Rural 50 (2020), https://doi.org/10.1590/0103-8478cr20190644.
[15] F. Kozisek, Regulations for calcium, magnesium or hardness in drinking water in the European Union member states, Regul. Toxicol. Pharm. 112 (2020), https://doi.org/10.1016/j.yrtph.2020.104589 104589.
[16] S. Faisal, S. Farooq, G. Hussain, E. Bashir, Influence of hard water on solubility and colorimetric properties of reactive dyes, AATCC J. Res. 6 (2019) 1–6.
[17] C. Yang, Factors affecting the accuracy of titration calcium carbonate content, Chem. Eng. Des. Commun. (2018) 126.
[18] A.B. dos Santos, K.A. Kohlmeier, M.E. Rocha, G.E. Barreto, J.A. Barreto, A.C.A. de Souza, M.A. Bezerra, Hair in Parkinson's disease patients exhibits differences in Calcium, Iron and Zinc concentrations measured by flame atomic absorption spectrometry– FAAS, J. Trace Elem. Med. Bio. 47 (2018) 134–139, https://doi.org/10.1016/j.jtemb.2018.02.003.
[19] D.J. Butcher, Recent advances in the determination of calcium and its use as an internal standard in environmental samples: fundamentals and applications, Appl. Spectrosc. Rev. 55 (2020) 60–75, https://doi.org/10.1080/05704928.2019.1570520.
[20] X. Fu, K. Xu, X. Feng, B. Chang, F. Yang, R. Huang, CaCO 3 nanoparticles as the tags for potentiometric detection of a cardiac biomarker using a calcium ion-selective electrode, Anal. Methods-UK 9 (2017) 6609–6612, https://doi.org/10.1039/c7ay01949a.
[21] J. Shu, D.J.A.C. Tang, Recent advances in photoelectrochemical sensing: from engineered photoactive materials to sensing devices and detection modes, Anal. Chem. 92 (2019) 363–377, https://doi.org/10.1021/acs.analchem.9b04199.
[22] O.D. Supekar, D.J. Park, A.R. Greenberg, J.T. Gopinath, V.M. Bright, Real-time detection of early-stage calcium sulfate and calcium carbonate scaling using Raman spectroscopy, J. Membrane Sci. 596 (2020), https://doi.org/10.1016/j.memsci.2019.117603 117603.

[23] B. Zhang, B. Liu, D. Tang, R. Niessner, G. Chen, D.J.A.c. Knopp, DNA-based hybridization chain reaction for amplified bioelectronic signal and ultrasensitive detection of proteins, Anal. Chem. 84 (2012) 5392–5399, https://doi.org/10.1021/ac3009065.
[24] J. Tang, D. Tang, R. Niessner, G. Chen, D.J.A.c. Knopp, Magneto-controlled graphene immunosensing platform for simultaneous multiplexed electrochemical immunoassay using distinguishable signal tags, Anal. Chem. 83 (2011) 5407–5414, https://doi.org/10.1021/ac200969w.
[25] Q. Wu, N. Li, Y. Wang, Y. Xu, J. Wu, G. Jia, F. Ji, X. Fang, F. Chen, X. Cui, Ultrasensitive and selective determination of carcinoembryonic antigen using multifunctional ultrathin amino-functionalized Ti3C2-MXene nanosheets, Anal. Chem. 92 (4) (2020) 3354–3360, https://doi.org/10.1021/acs.analchem.9b05372.
[26] J. Tang, D. Tang, R. Niessner, G. Chen, D. Knopp, Magneto-controlled graphene immunosensing platform for simultaneous multiplexed electrochemical immunoassay using distinguishable signal tags, Anal. Chem. 83 (13) (2011) 5407–5414, https://doi.org/10.1021/ac200969w.
[27] Q. Zhang, Y. Cai, H. Li, D.-M. Kong, H.-X.J.B. Shen, Bioelectronics, Sensitive dual DNAzymes-based sensors designed by grafting self-blocked G-quadruplex DNAzymes to the substrates of metal ion-triggered DNA/RNA-cleaving DNAzymes, Biosens. Bioelecron. 38 (2012) 331–336, https://doi.org/10.1016/j.bios.2012.06.011.
[28] J. Zhuang, L. Fu, M. Xu, Q. Zhou, G. Chen, D.J.B. Tang, Bioelectronics, DNAzyme-based magneto-controlled electronic switch for picomolar detection of lead (II) coupling with DNA-based hybridization chain reaction, Biosens. Bioelecron. 45 (2013) 52–57, https://doi.org/10.1016/j.bios.2013.01.039.
[29] D. Tang, B. Xia, Y. Tang, J. Zhang, Q.J.M.A. Zhou, Metal-ion-induced DNAzyme on magnetic beads for detection of lead (II) by using rolling circle amplification, glucose oxidase, and readout of pH changes, Microch. Acta 186 (2019) 318, https://doi.org/10.1007/s00604-019-3454-1.
[30] W. Zhou, R. Saran, Q. Chen, J. Ding, J.J.C. Liu, A new Na^{+}-Dependent RNA-cleaving DNAzyme with over 1000-fold rate acceleration by ethanol, ChemBioChem 17 (2016) 159–163, https://doi.org/10.1002/cbic.201500603.
[31] X. Fan, H. Li, J. Zhao, F. Lin, L. Zhang, Y. Zhang, S.J.T. Yao, A novel label-free fluorescent sensor for the detection of potassium ion based on DNAzyme, Talanta 89 (2012) 57–62, https://doi.org/10.1016/j.talanta.2011.11.056.
[32] R. Saran, J.J.A.c. Liu, A silver DNAzyme, Anal. Chem. 88 (2016) 4014–4020.doi, https://doi.org/10.1021/acs.analchem.6b00327.s001.
[33] D. Zhou, W. Wu, Q. Li, J. Pan, J.J.A.M. Chen, A label-free and enzyme-free aptasensor for visual Cd^{2+} detection based on split DNAzyme fragments, Anal. Methods-UK 11 (2019) 3546–3551, https://doi.org/10.1039/c9ay00822e.
[34] H. Wang, Y. Liu, G.J.A.s. Liu, Electrochemical biosensor using DNA embedded phosphorothioate modified RNA for mercury ion determination, ACS sensors 3 (2018) 624–631, https://doi.org/10.1021/acssensors.7b00892.s001.
[35] H. Wei, B. Li, J. Li, S. Dong, E. Wang, DNAzyme-based colorimetric sensing of lead (Pb2+) using unmodified gold nanoparticle probes, Nanotechnology 19 (9) (2008), https://doi.org/10.1088/0957-4484/19/9/095501 095501.
[36] S. Liu, C. Cheng, H. Gong, L.J.C.C. Wang, Programmable Mg^{2+}-dependent DNAzyme switch by the catalytic hairpin DNA assembly for dual-signal amplification toward homogeneous analysis of protein and DNA, Chem. Commun. 51 (2015) 7364–7367, https://doi.org/10.1039/c5cc01649e.
[37] K.E. Nelson, P.J. Bruesehoff, Y.J.J.o.m.e. Lu, In vitro selection of high temperature Zn^{2+}-dependent DNAzymes, J. Mol. Evol. 61 (2005) 216–225, https://doi.org/10.1007/s00239-004-0374-3.
[38] H. Wang, Y. Liu, J. Wang, B. Xiong, X.J.M.A. Hou, Electrochemical impedance biosensor array based on DNAzyme-functionalized single-walled carbon nanotubes using Gaussian process regression for Cu (II) and Hg (II) determination, Microch. Acta 187 (2020) 1–9, https://doi.org/10.1007/s00604-020-4202-2.
[39] S. Ghosh, Y. Chen, A. George, M. Dutta, M.A.J.F.i.C. Stroscio, fluoropescence resonant energy transfer-based quantum dot sensor for the detection of calcium ions, Front. Chem. 8 (2020) 594, https://doi.org/10.3389/fchem.2020.00594.
[40] I. Heaton, M.J.S. Platt, DNAzyme sensor for the detection of Ca^{2+} using resistive pulse sensing, Sensors-Basel 20 (2020) 5877, https://doi.org/10.3390/s20205877.
[41] V.K. Gupta, A.K. Singh, L.K. Kumawat, N.J.S. Mergu, A.B. Chemical, An easily accessible switch-on optical chemosensor for the detection of noxious metal ions Ni(II), Zn(II), Fe(III) and UO_2(II), Sensor. Actuat. B-Chem. 222 (2016) 468–482, https://doi.org/10.1016/j.snb.2015.08.063.
[42] W. Zhou, R. Saran, P.J.J. Huang, J. Ding, J.J.C. Liu, An exceptionally selective DNA cooperatively binding two Ca^{2+} ions, ChemBioChem. 18 (2017) 518–522, https://doi.org/10.1002/cbic.201600708.
[43] R. Laref, E. Losson, A. Sava, M. Siadat, On the optimization of the support vector machine regression hyperparameters setting for gas sensors array applications.", Chemometr Intell. Lab. (2019) 22–27, https://doi.org/10.1016/j.chemolab.2018.11.011.
[44] I. Pisa, I. Santín, J.L. Vicario, A. Morell, R. Vilanova, ANN-based soft sensor to predict effluent violations in wastewater treatment plants, Sensors 19 (6) (2019) 1280, https://doi.org/10.3390/s19061280.
[45] H. Wang, S. Zheng, X. Nan, Y. Zhao, Y. Wang, F. Zhang, L. Yang, L. Xu, B. Xiong, Non-specific DNAzyme-based biosensor with interfering ions for the Cd^{2+} determination in feed, Sensor. Actuat. B-Chem. (2020), https://doi.org/10.1016/j.snb.2020.12913 129139.
[46] H. Wang, Y. Yin, L.J.E. Gang, Single-gap microelectrode functionalized with single-walled carbon nanotubes and Pbzyme for the determination of Pb^{2+}, Electroanl. 31 (2019) 1174–1181, https://doi.org/10.1002/elan.201900016.